






## Article

# Bioenergetic Profiling in Glioblastoma Multiforme Patients with Different Clinical Outcomes

Vivi Bafiti <sup>1</sup>, Sotiris Ouzounis <sup>1</sup>, Eleni Siapi <sup>1</sup>, Ioanna Maria Grypari <sup>2</sup>, Andreas Theofanopoulos <sup>3</sup>, Vasilios Panagiotopoulos <sup>3</sup>, Vasiliki Zolota <sup>2</sup>, Dimitrios Kardamakis <sup>4</sup> and Theodora Katsila <sup>1,\*</sup>

<sup>1</sup> Institute of Chemical Biology, National Hellenic Research Foundation, 11635 Athens, Greece

<sup>2</sup> Department of Pathology, School of Medicine, University of Patras, 26504 Patras, Greece

<sup>3</sup> Department of Neurosurgery, University Hospital of Patras, 26504 Patras, Greece

<sup>4</sup> Department of Radiation Oncology, University of Patras Medical School, 26504 Patras, Greece

\* Correspondence: thkatsila@eie.gr; Tel.: +30-210-7273-752

**Abstract:** The accumulation of cell biomass is associated with dramatically increased bioenergetic and biosynthetic demand. Metabolic reprogramming, once thought as an epiphenomenon, currently relates to disease progression, also in response to extracellular fate-decisive signals. Glioblastoma multiforme patients often suffer misdiagnosis, short survival time, low quality of life, and poor disease management options. Today, tumor genetic testing and histological analysis guide diagnosis and treatment. We and others appreciate that metabolites complement translational biomarkers and molecular signatures in disease profiling and phenotyping. Herein, we coupled a mixed-methods content analysis to a mass spectrometry-based untargeted metabolomic analysis on plasma samples from glioblastoma multiforme patients to delineate the role of metabolic remodeling in biological plasticity and, hence, disease severity. Following data processing and analysis, we established a bioenergetic profile coordinated by the mitochondrial function and redox state, lipids, and energy substrates. Our findings show that epigenetic modulators are key players in glioblastoma multiforme cell metabolism, in particular when microRNAs are considered. We propose that biological plasticity in glioblastoma multiforme is a mechanism of adaptation and resistance to treatment which is eloquently revealed by bioenergetics.

**Keywords:** untargeted metabolomics; glioblastoma multiforme; translational biomarkers; bioenergetics; oncometabolism; metabolic reprogramming; epigenetic modulators; drug repurposing



**Citation:** Bafiti, V.; Ouzounis, S.; Siapi, E.; Grypari, I.M.; Theofanopoulos, A.; Panagiotopoulos, V.; Zolota, V.; Kardamakis, D.; Katsila, T. Bioenergetic Profiling in Glioblastoma Multiforme Patients with Different Clinical Outcomes. *Metabolites* **2023**, *13*, 362. <https://doi.org/10.3390/metabo13030362>

Academic Editors: Olga Papadodima and Konstantinos Voutetakis

Received: 1 February 2023

Revised: 20 February 2023

Accepted: 23 February 2023

Published: 28 February 2023



**Copyright:** © 2023 by the authors. Licensee MDPI, Basel, Switzerland. This article is an open access article distributed under the terms and conditions of the Creative Commons Attribution (CC BY) license (<https://creativecommons.org/licenses/by/4.0/>).

## 1. Introduction

Glioblastoma multiforme (GBM), a World Health Organization (WHO) grade IV central nervous system (CNS) tumor, is characterized by intra-tumoral heterogeneity and inter-individual variability, which are key determinants of disease progression and low survival rates (average survival time of 12–15 months) [1–3]. The current—and since almost two decades—first line standard of care for GBM includes surgical resection followed by adjuvant, fractionated radiotherapy (RT) with concomitant and maintenance temozolomide (TMZ) chemotherapy [3–5]. Diagnosis and recurrence monitoring are routinely carried out by computed tomography and magnetic resonance imaging modalities, yet their application is limited when it comes to large-scale screening due to radiation side effects, cost, and, sometimes, inaccessibility. Alternatives of clinical utility and, at the same time, clinical validity are missing as tumor biopsy-based strategies (such as fine needle aspiration biopsy and genetic profiling or sequencing of circulating tumor DNA) are themselves too invasive in nature for repeated sampling [6,7]. Liquid biopsy-methods are emerging as they are accompanied by technological advances in both dry- and wet-lab approaches [8,9]; however, they are not ready for prime-time, when the unmet needs are listed either for the general public or GBM patients.

Metabolomics has come forward as a prevailing analytical strategy that maps holistically the molecular status in a given biological sample informing about the interplay of the genome and environmental influences. Such individual profiles (metabotypes) serve as snapshots, which are extremely informative in nature as they are the net result of tumor and host biology in the presence of xenobiotics. Therefore, metabolomics datasets not only allow for hypothesis-driven data interpretation, but also the generation of hypotheses. Of note, metabotypes may complement other omics data layers (metabolomics-based multi-omics) and/or predict response to treatment via mathematical modeling (pharmacometabolomics).

Metabolic reprogramming, a hallmark of cancer, is involved in tumor aggressiveness and treatment resistance allowing for tumor cells to adapt to their bioenergetic and biosynthetic demands [10]. In GBM, tumors appear to manipulate and exploit normal brain cells, affecting almost all cell types at the tumor niche via intracellular biological plasticity and multiple types of communication [11]. Thus, we and others map the genome-environment interplay with high time sensitivity and spatial resolution via multi-omics as a key strategy for precision oncology [12,13].

Efforts to map the GBM metabolic landscape are multi-level (tumor, tumor niche, biofluids). Key cell metabolism alterations in GBM relate to disordered lipid metabolism, dysfunctional oxidative phosphorylation, and increased Warburg effect [14,15]. Recently, the role of epigenetic modulators as regulators in tumor cell metabolism has gained great interest. Such epigenetic modulators include histone modifications, DNA methylation, nucleosome remodeling, and non-coding RNAs (long-noncoding RNAs, circular RNAs, microRNAs) [16,17]. In particular, microRNAs act as regulators of metabolic gene expression either directly or by regulating metabolism-associated oncogenic signaling pathways, oncogenes, or tumor suppressors. In gliomas, microRNAs have been reported to target mRNAs of enzymes that participate in glycolysis, oxidative phosphorylation, lipid metabolism, and mitochondrial energy metabolism as well as glutamine metabolism [18,19]. To name but a few, Alfardus et al. reported miR-619-5p, miR-4440, and miR-4793-3p regulating lipid metabolic pathways in GBM [20], while Kwak et al. identified miR-3189 and its role in glucose metabolism by targeting GLUT3 in GBM cell lines [21]. Oncogenic K-Ras, EGFR, c-myc, and mTORC2 as well as PI3K/Akt and LKB1-AMPK pathways are also regulated by microRNAs [14].

Up to now, only a limited number of studies have explored the metabolic landscape of GBM patients focusing on biofluids in line with the anticipation that the latter will pave the way towards non-invasive procedures in the clinic, despite the advantage of untargeted mass spectrometry-based metabolomics to detect as many metabolites as possible at once, identify unexpected metabolic alterations, and characterize novel metabolites in biological samples [12,22–25]. Even fewer are the datasets that are well-balanced both at the exploratory and validation phases [26,27] coupling untargeted metabolomics to a mixed-methods content analysis.

Herein, we designed, employed, and optimized a strategy coupling a mixed-methods content analysis (i.e., gold standard approach for content analysis) to a metabotype approach for GBM patients to delineate the role of metabolic remodeling in biological plasticity and, hence, disease severity. For this, GBM bioenergetic profiles were explored at the time of diagnosis and during follow-up (GBM patients,  $n = 21$ ; plasma samples,  $n = 122$ ). Next, the informative relationships through which metabolites are connected were interrogated. This holistic strategy presents a great opportunity to unveil patterns and provide new insights for GBM biology and drug repurposing.

## 2. Materials and Methods

### 2.1. Mixed-Methods Content Analysis

We employed a mixed-methods content analysis, a gold standard approach for a content analysis that consists of deductive (quantitative) and inductive (qualitative) phases, while contemporary definitions are considered. For data and text mining as well as data analysis, peer-reviewed literature, omics datasets, and clinical trial outcomes (as

of 2022) were mined to interrogate GBM plasma metabolotypes. We have also developed a novel framework to meet our analytical demands, exploring data (both context and content). Literature data from Scopus and PubMed/MEDLINE were queried. Scopus and PubMed/MEDLINE are the largest citation and abstract databases of peer-reviewed literature. To account for selection biases, private and publicly available texts have been assessed (based on the inclusion/exclusion criteria set). Keywords and MeSH terms ([www.nlm.nih.gov/mesh](http://www.nlm.nih.gov/mesh), accessed on 23 January 2020) included “GBM OR glioblastoma AND plasma AND metabolomics”, “GBM OR glioblastoma AND untargeted metabolomics”, and “GBM OR glioblastoma AND metabolotypes”. We questioned the interim output further for open data (yes/no), sample size (validated by a power analysis), research approach, and publication impact/metrics. Studies that failed to meet inclusion criteria or studies on non-human samples were excluded. Two co-authors (V.B. and T.K.) co-analyzed the interim and final outputs, and then, the percentage of inter-rater agreement was calculated. To account for biases, Cohen’s kappa statistic and percentage agreement were also determined with multi-categorical ratings.

To interrogate further GBM plasma metabolotypes as well as the informative relationships through which metabolites are connected, we queried the Human Metabolome Database (HMDB) [28], the Metabolomics Workbench, <https://www.metabolomicsworkbench.org/>, (accessed on 9 October 2020, 9 October 2021 and 29 December 2022), and Metabolights [29].

## 2.2. Clinical Cohort and Samples

The study protocol is in accordance with the Declaration of Helsinki and has been approved by the ethics review board of the General University Hospital of Patras, Greece. IRB protocol number: 8735/142. Study participants signed a written informed consent. Patients ( $n = 21$ ) have received the diagnosis of GBM based on the WHO criteria applicable at the time of recruitment (according to the WHO classifications of 2016 and 2021), and the standard-of-care treatment protocol was applied [3,30]. Overall survival (OS) was determined from the time of diagnosis until death or last follow-up (12 months). Clinical and demographic characteristics are shown in Table S1.

## 2.3. Untargeted Metabolomics

### 2.3.1. Sample Preparation

Sample collection, processing, and storage for both blood and plasma samples ( $n = 122$ ) were performed as described in Chalikiopoulou et al. [31]. For LC-MS-based untargeted metabolomics analysis, plasma samples were thawed on ice at 4 °C, and 400  $\mu$ L of plasma were aliquoted into a 2.0 mL low-adherence microcentrifuge tube. Sample extraction was carried out by ice-cold methanol (3:1) ( $v/v$ ) for best metabolite yield, and then, the mixture was vortexed for 15 s. Samples were centrifuged at  $15,800 \times g$  for 15 min at room temperature to pellet the protein precipitate. The supernatant was transferred into a new 1.5 mL low-adherence microcentrifuge tube and dried down (lyophilized) in a centrifugal vacuum evaporator for 18 h. No heating was applied during the drying process. Next, samples were reconstituted with 180  $\mu$ L 80:20 methanol in water ( $v/v$ ), sonicated for 10 min, and centrifuged for 1 min at  $14,000 \times g$  (room temperature). The 100  $\mu$ L-aliquots were transferred to each insert of liquid chromatography (LC) glass vial, N8. Quality control (QC) and internal standard (IS) samples were prepared as described in Chalikiopoulou et al. [31].

### 2.3.2. Chromatographic Conditions

The liquid chromatography separation was performed with an Accela ultra-high-performance LC (UHPLC) system. A polymeric SeQuant<sup>®</sup> ZIC<sup>®</sup>-pHILIC column (5  $\mu$ m, 150 mm  $\times$  2.1 mm) (150,460, Merck) and a SeQuant<sup>®</sup> ZIC<sup>®</sup>-pHILIC Guard Kit (20  $\times$  2.1 mm) (50,438, Merck) were used operating at 45 °C. The injection mode was set at 5  $\mu$ L, and the mobile phase flow rate was set at 0.3 mL/min. Mobile phase solvents were A (95% H<sub>2</sub>O, 5% methanol, 0.1% formic acid) and B (100% methanol). The eluting gradient program in both

positive and negative ion mode was the following: 0–1.0 min (95% A, 5% B), 1.0–4.0 min (45% A, 55% B), 4.0–9.0 min (45% A, 55% B), 9.0–10.0 min (20% A, 80% B), 10.0–10.1 min (20% A, 80% B), 10.1–15.0 min (0% A, 100% B), 15.0–15.1 min (0% A, 100% B), and 15.1–20.0 min (95% A, 5% B).

### 2.3.3. Mass Spectrometry

The UHPLC system was coupled to an LTQ-Orbitrap Velos mass spectrometer (Thermo Fisher Scientific, Bremen, Germany) equipped with an APCI source, operating in both positive and negative modes. To monitor the instrument performance over time and chromatographic integrity, including retention time shifts, QC samples were prepared as a mix of each sample. Data were pre-processed with Xcalibur software (version 2.1, Thermo Scientific, Waltham, MA, USA).

### 2.3.4. Data Processing and Statistical Analysis

Data processing and analysis were performed as described in Chalikiopoulou et al. [31]. ProteoWizard MSConvert [32] was used to centroid all raw MS data and convert them into MzML files prior to MetaboAnalyst 5.0 [33]. LC-MS spectral processing was performed using the auto-optimized parameter setting and blank subtraction. All test-groups were cross-compared, first to gain insights into the GBM metabolomes and then to identify key metabolites. Both positive and negative ion modes were employed during LC-MS analysis. Subsequent analyses included metabolites detected in more than 33% of the samples. Following the removal of uninformative features, the resulting number of metabolites was decreased drastically to  $\sim 1/4$ . For those metabolites surviving our criteria, empty values were annotated with a small value (1). Data centering and unit variance scaling were carried out. Univariate and multivariate statistical analysis were applied where appropriate. Student's *t*-test and ANOVA (One-way Analysis of Variance) test followed by post hoc analysis (Fisher's least significant difference) were used. Critical value was set at  $<0.05$ , including FDR correction. For all comparative analysis, we performed Log2fold calculation and PCA and PLS analyses. Next, we determined PLS VIP (variable importance in projection) values. Only metabolites with a  $\log_2\text{fold} \geq 2$  were selected for subsequent enrichment analysis. Enrichment analysis was performed using Metaboanalyst 5.0 [33] employing pathway-associated metabolite sets (SMPDB). For the interrogation of metabolic pathways, the mummichog algorithm was applied. This algorithm facilitates one-step functional analysis through tandem mass spectra feature tables [34]. The top 10 most significantly associated *m/z* features were used as input to the mummichog algorithm v.2. KEGG (Kyoto Encyclopedia of Genes and Genomes) database was selected as the pathway library of interest. Only those metabolic pathways containing at least 3 significant metabolites were included. Significance threshold was set at a *p*-value  $< 0.05$ , including FDR correction.

## 2.4. Machine Learning

### 2.4.1. Supervised Machine Learning

To evaluate the predictive value of those metabolites that have statistically significant differences in their levels between low-risk (OS > 12 months; *n* = 11) and high-risk (OS < 12 months; *n* = 10) groups, a discriminant analysis was implemented. A supervised machine learning approach was employed, and hence, several classifiers were tested to find which can model best metabolite levels. Algorithms were trained to stratify patients to either low-risk or high-risk groups based on seven metabolites: perlolyrine, piperidine, hippuric acid, 2,6-diisopropyl-3-methylphenol, dopamine, 7-ketocholesterol, and ( $\pm$ )-(Z)-2-(5-tetradecenyl)cyclobutanone. Metabolites were pre-processed and normalized, before being fed to the classification scheme. To assess the predictive ability of metabolite combinations, Recursive Feature Elimination (RFE) [35] was applied. This feature selection method was evaluated through 10-fold cross validation. Next, four classifiers were trained: SVM [36], Random Forest (RF) [37], eXtreme Gradient Boosting (XGBoost) [38],

and Stochastic Gradient Boosting (GBM) [39]. Taking into account sample size and external test feasibility, we opted for a 10-fold cross validation method to evaluate the predictive ability of the algorithms tested as well as the robustness of the models. The metrics that were used for the evaluation of the models were:

$$\text{Accuracy} = \frac{\text{TP} + \text{TN}}{\text{TP} + \text{TN} + \text{FP} + \text{FN}}$$

$$\text{Sensitivity} = \frac{\text{TP}}{\text{TP} + \text{FN}}$$

$$\text{Specificity} = \frac{\text{TN}}{\text{TN} + \text{FP}}$$

$$\text{Matthews Correlation Coefficient} = \frac{\text{TP} \times \text{TN} - \text{FP} \times \text{FN}}{\sqrt{(\text{TP} + \text{FP})(\text{TP} + \text{FN})(\text{TN} + \text{FP})(\text{TN} + \text{FN})}}$$

$$\text{F1 score} = \frac{2\text{TP}}{2\text{TP} + \text{FP} + \text{FN}}$$

where TP indicates the case of a high-risk patient who is correctly classified, and TN denotes the correctly identified low-risk patients by the models. FN corresponds to the case of a high-risk patient who is wrongly predicted as low-risk, and FP denotes the case of a low-risk patient who is classified as high-risk by the models. Next, an analysis of feature importance was implemented to identify which metabolites mostly affect the prediction in question for the model with the optimal performance. The analysis was performed in Rstudio using caret library for machine learning [40].

#### 2.4.2. Unsupervised Machine Learning

An unsupervised method may provide an unbiased indication about whether the integration of miRNA data and metabolotypes could have a predictive value. Thus, an unsupervised machine learning approach was also implemented for the validation of the predictive value for the seven metabolites that stratify low- and high-risk patients (perlolyrine, piperidine, hippuric acid, 2,6-diisopropyl-3-methylphenol, dopamine, 7-ketocholesterol, ( $\pm$ )-(Z)-2-(5-tetradecenyl)cyclobutanone). For this, we focused on a cluster analysis for a sub-population of the GBM cohort sharing both miRNA (hsa-miR-20a, hsa-miR-21, hsa-miR-10a) [41] and untargeted metabolomics datasets (n = 7; low-risk, n = 4; high-risk, n = 3). The clustering algorithms used were k-means (k was set to two) [42] and hierarchical clustering [43]. All analyses were carried out with the R programming language.

### 3. Results

#### 3.1. Untargeted Metabolomics Suggest Metabolic Remodeling Patterns in GBM Patients with Different Clinical Outcomes and Response to Treatment

The interrogation of GBM plasma metabolotypes as well as the informative relationships through which metabolites are connected by our mixed-methods content analysis, followed by queries in the Human Metabolome Database (HMDB) [28], the Metabolomics Workbench, <https://www.metabolomicsworkbench.org/> (accessed on 9 October 2020, 9 October 2021 and 29 December 2022) and Metabolights (MTBLS858, MTBLS730, MTBLS3873, MTBLS1558, MTBLS4708) [29] revealed data scarcity and sparsity. There were no available cohorts of low-risk vs. high-risk at diagnosis and during RT + TMZ follow-up neither mass spectrometry-based untargeted metabolomics datasets for plasma. This has been a rather unfortunate outcome despite it adds value to our study presented herein.

Our RT + TMZ patient cohort demonstrated no age- or sex-dependence. Molecular-clinical correlations were drawn to classify low-risk (OS > 12 months) vs. high-risk (OS < 12 months) GBM patients; 52% (n = 11) and 48% (n = 10) were assigned to low- and high-risk groups, respectively.

Untargeted GBM plasma metabolomics enabled relative quantitative analysis with a high degree of confidence resulting in the annotation and quantification of 1545 metabolites.

When comparing the low- to high-risk groups by univariate analysis,  $n = 38$  metabolites were significantly modulated (adjusted  $p$ -value  $< 0.05$ ), while  $n = 30$  metabolites exhibited fold change values (FC)  $> 2.0$ . The metabolotypes of the low-risk patients consist of increased levels of perlolyrine, piperidine, 2,6-diisopropyl-3-methylphenol, dopamine, and 7-ketocholesterol, whereas higher levels of ( $\pm$ )-(Z)-2-(5-Tetradecenyl)cyclobutanone and hippuric acid are noted for high-risk patients (Figure 1). Despite being small, significant correlations are found between the known patient characteristics and quantified metabolites.

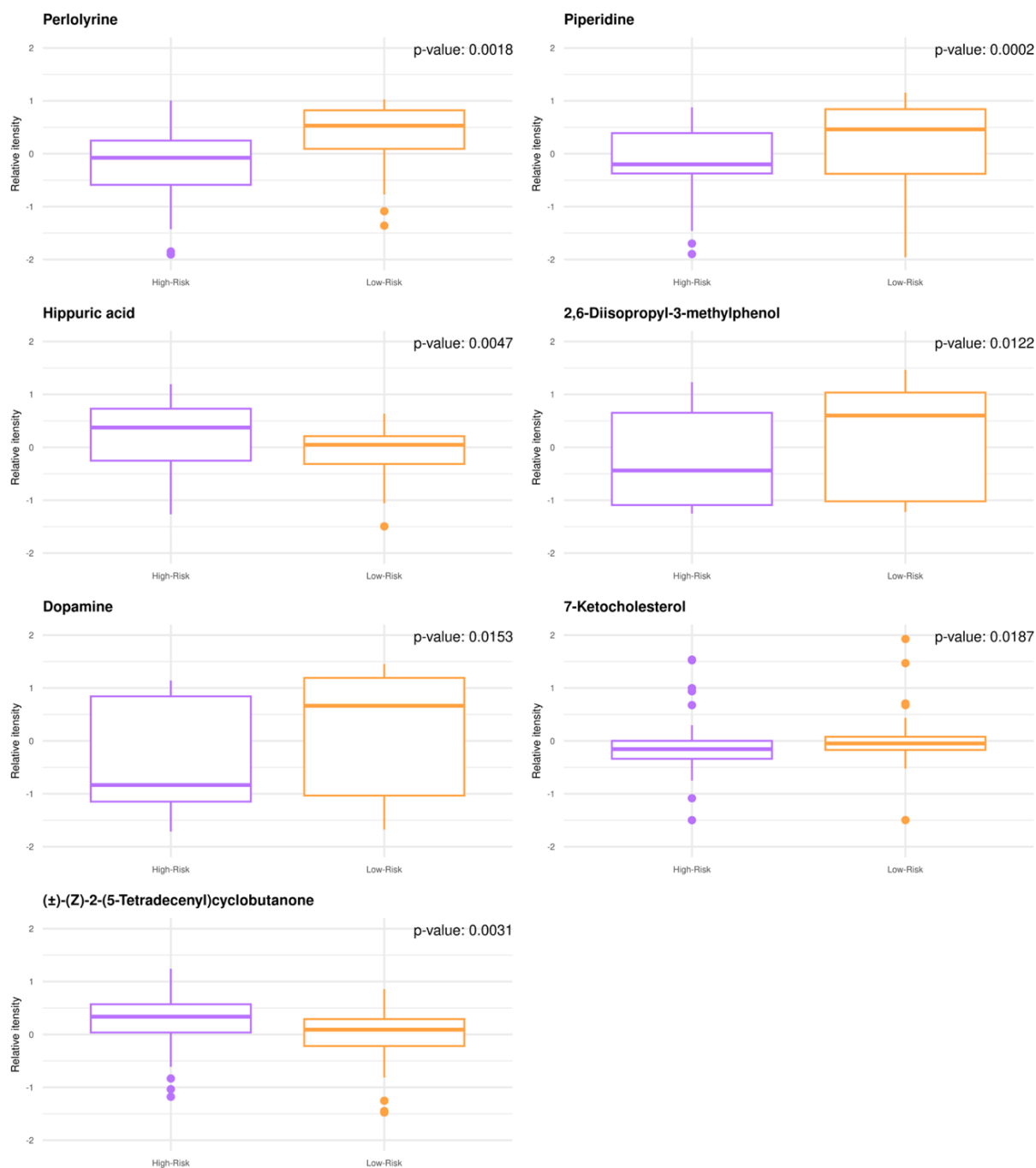


**Figure 1.** GBM plasma metabolotypes enable risk stratification (low-risk, OS  $> 12$  months; high-risk, OS  $< 12$  months). Boxplots of the annotated metabolites with (FC)  $> 2.0$  and  $p$ -value  $< 0.05$ . Individual dots serve as a visual representation of data distribution (such values when inter-individual variability is considered are important features of the data to be analyzed and interpreted). Group comparisons are color-coded: purple, high-risk; orange, low-risk.

Additional metabolite changes detected refer to aminoacids, lipids, mitochondrial energy metabolism, and energy substrates. Such metabolic alterations were found when low-risk GBM plasma metabolotypes were compared to their high-risk counterparts (group comparison-a) or when baseline GBM plasma metabolotypes were compared to those after first RT + TMZ (group comparison-b). For group comparison-a, the most prominent ones, sharing FC > 2.0, yet showing no statistical significance or being statistically significant with FC < 2.0 were: alanine, valine, pyroglutamic acid, 3-methylene-indolenine, and indoxyl. For group comparison-b, acetylphosphate, thymine, histidine, pentadecanoic acid, N-undecanoylglycine, linoleic acid, 3-Methylene-indolenine, tyrosine, and alanylproline were among the most prominent ones.

To explore metabolic remodeling patterns when considering response to treatment (RT + TMZ) in addition to clinical outcomes (OS), one-way ANOVA test and post hoc analysis were conducted, comparing low-risk patients at the time of diagnosis vs. low-risk patients after first RT + TMZ vs. high-risk patients at the time of diagnosis vs. high-risk patients after first RT + TMZ (Figure 2). 2-acetyl-4-methylpyridine, piperidine, and 3-(4-methyl-3-pentenyl)thiophene were revealed as those significantly modulated among test-groups. Of note, the relative intensity of piperidine appeared to have lower mean values in high-risk patients at the time of diagnosis as well as following first RT + TMZ empowering risk stratification and response to treatment. When interrogating GBM plasma metabolotypes during disease progression after therapeutic intervention, independently of risk-groups, there was no statistically significant outcome after false discovery rate (FDR) correction.



**Figure 2.** Modulation of metabolites in low-risk patients (OS > 12 months) vs. high-risk (OS < 12 months) GBM patients, at the time of diagnosis (baseline) and after first RT + TMZ. Boxplots of top-metabolites (adjusted  $p$ -value < 0.05). Individual dots serve as a visual representation of data distribution (such values when inter-individual variability is considered are important features of the data to be analyzed and interpreted). Group comparisons; low-risk patients at the time of diagnosis vs. low-risk patients after first RT + TMZ vs. high-risk patients at the time of diagnosis vs. high-risk patients after first radiotherapy RT + TMZ.

### 3.2. GBM Plasma Metabotypes Are Indicative of Disease Severity

Aiming to explore further the metabotypes of the low- and high-risk GBM patients, functional enrichment analysis was performed, and the most perturbed metabolic pathways

were highlighted (adjusted  $p$ -value < 0.03; enrichment ratio > 2.0). Data are summarized in Figure 3A.

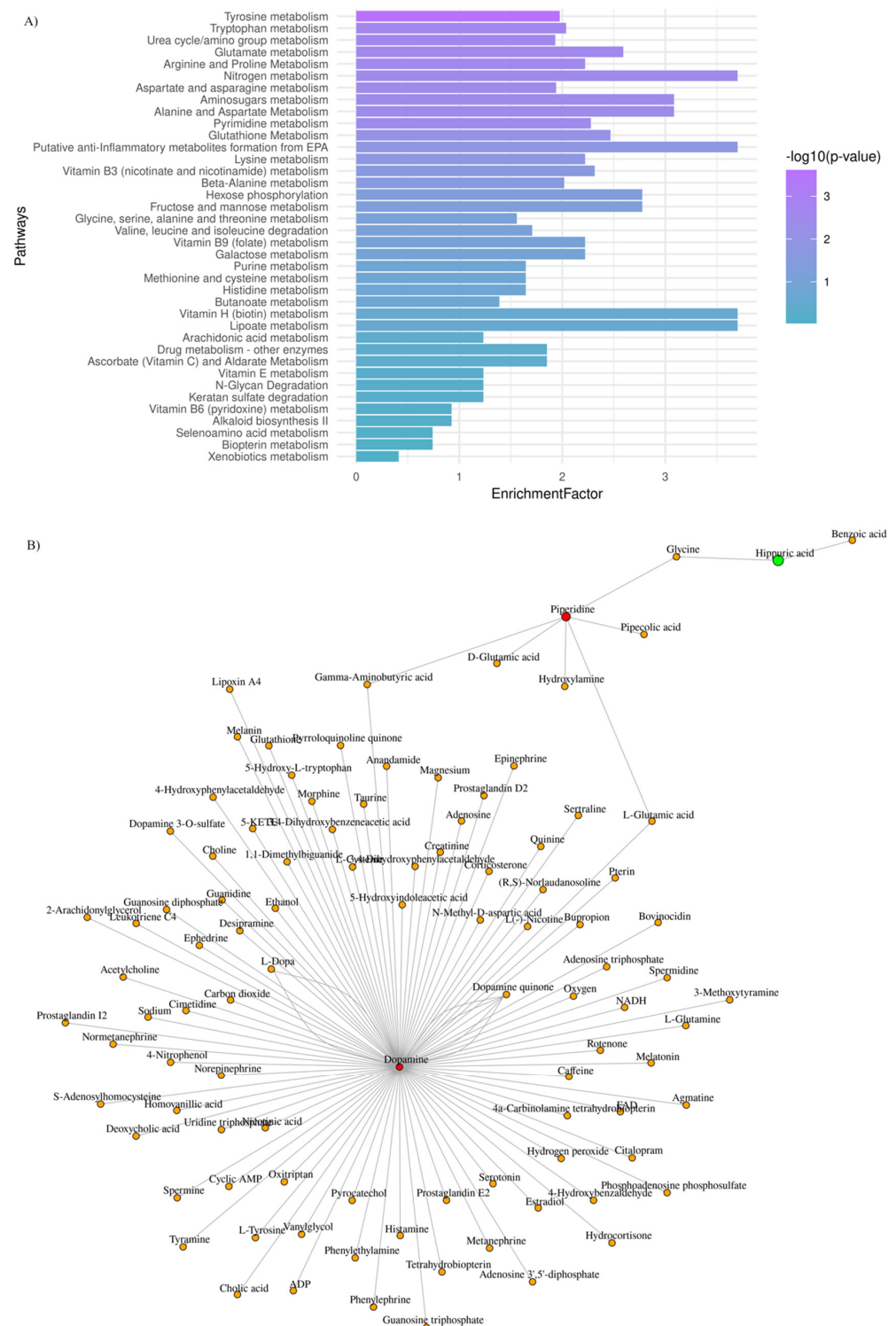


**Figure 3.** GBM plasma metabolites reveal metabolic dysregulation that reflects disease severity. (A) Mummichog functional analysis was carried out by MetaboAnalyst v.5. Enriched pathways were ranked by significance (see color scale); (B) Metabolite-metabolite interaction network of metabolites whose levels are significantly increased (red) and decreased (green), when low-risk vs. high-risk GBM patients are considered.



To draw functional relationships for the test-groups in question, we constructed a subgraph for those metabolites that exhibited  $(FC) > 2$  by querying the KEGG knowledge-based network. As shown in Figure 3B, we identified a subnetwork that consists of dopamine, piperidine, and hippuric acid (99 nodes; 104 edges). Dopamine presented the highest degree value (degree value of 96), which indicates the number of direct neighbors as well as the highest value of betweenness centrality (betweenness of 4717.5), which corresponds to the shortest paths going through this metabolite. Our mixed-methods content analysis was also employed for data interpretation to avoid selection biases.

### 3.3. GBM Plasma Metabotypes Enable Low- and High-Risk Predictions

A predictive value for perlolyrine, piperidine, hippuric acid, 2,6-diisopropyl-3-methylphenol, dopamine, and  $(\pm)$ -(Z)-2-(5-Tetradecenyl) cyclobutanone was obtained by discriminant analysis based on GBM plasma metabotypes and feature selection analysis (82% accuracy) (Figure S1). Gradient boosting had the best performance and highest area under the curve (AUC) of 93.2%, whereas Random Forest had an AUC of 71.3% (Figure 4). The performance of all models after 10-fold cross validation is provided in Table S2. Gradient boosting had best performance metrics (84% accuracy), reflecting model ability to yield predictions. Matthews Correlation Coefficient suggested that both low- and high-risk patients can be equally predicted. This fact is also evident from the confusion matrix in Table S3, which shows the number of low- and high-risk patients predicted correctly. As shown by the variable importance analysis (Gradient boosting), the contribution of each metabolite in algorithm decisions was also identified (Figure S2). Thus, hippuric acid has the most powerful effect on the model.

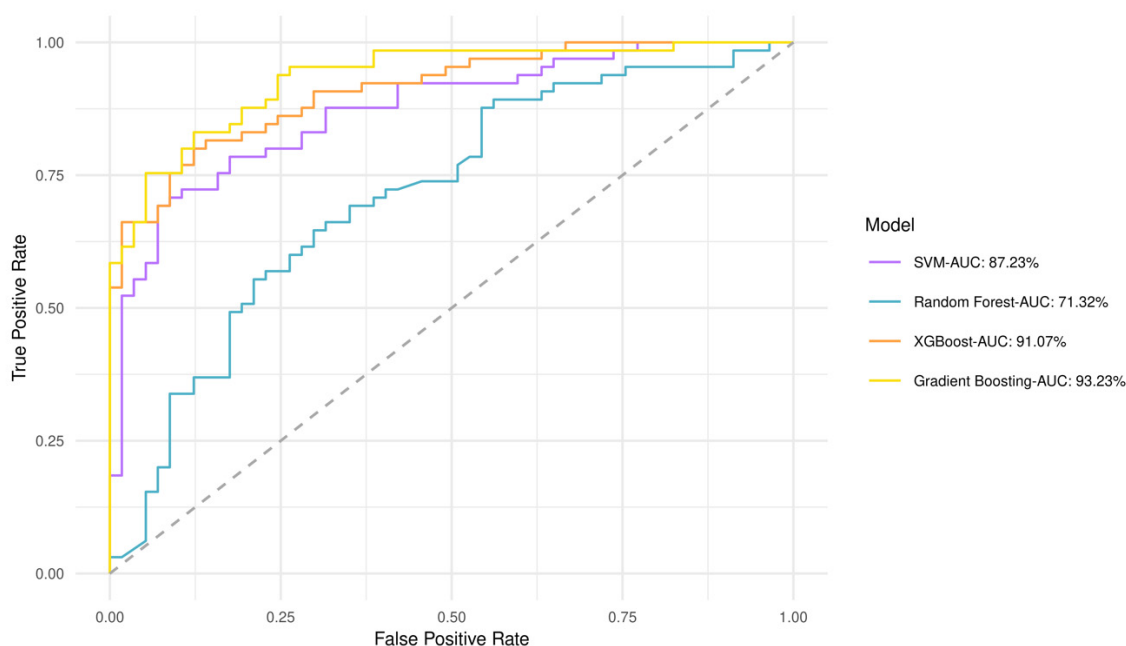


**Figure 4.** Receiver operating characteristic (ROC) curves and AUCs produced after 10-fold cross validation for the four classifiers trained to stratify low- and high-risk patients based on GBM plasma metabotypes.

Figures S3 and S4 suggest that both unsupervised models (k-means and hierarchical clustering) provide a discrimination accuracy equal to 86%, when miRNA (hsa-miR-20a, hsa-miR-21, hsa-miR-10a) data and metabotypes are integrated. Specificity is equal to 67% and 100% for the low- and high-risk groups, respectively.

#### 4. Discussion

Tumor heterogeneity and inter-individual variability are well-established GBM hallmarks, and hence, optimum decision-making post-diagnosis remains a challenge [44]. Deciphering GBM metabolotypes as direct indicators of those biochemical changes which define the disease phenotype of an individual may serve as a promising strategy to reveal unique features as well as the mechanistic interplay underlying the observed phenotypic and biological plasticity of GBM [45]. Herein, we employed mass spectrometry-based untargeted plasma metabolomics to gain insights into the rewired metabolic landscape of GBM patients with different clinical outcomes, response to treatment, and disease severity. To avoid selection biases, instead of a population-based estimate, taking into account the sample size of this study and the median OS, 12 months was the cut-off value set for the low- and high-risk groups, as also reported by pivotal studies (RT + TMZ) in GBM and/or clinical trials [46–48]. To this end, we also interrogated GBM plasma metabolotypes and the informative relationships through which metabolites are connected by a mixed-methods content analysis, followed by queries in the Human Metabolome Database (HMDB) [28], the Metabolomics Workbench, <https://www.metabolomicsworkbench.org/> (accessed on 9 October 2020, 9 October 2021 and 29 December 2022) and Metabolights (MTBLS858, MTBLS730, MTBLS3873, MTBLS1558, MTBLS4708) [29]. Data and text mining have been applied in cancer research to facilitate cancer systems biology [49], while Automated Metabolome Assembly has been presented in 2010 as the means to achieve a comprehensive system for metabolome prediction via a text-mining workflow [50].

Piperidine was found to be increased in low-risk GBM patients enabling risk stratification (Figure 1) and was identified among the top 3 metabolites that were significantly altered at the time of diagnosis (baseline) and following the first cycle of radiotherapy(+TMZ) (Figures 1 and 2). This metabolite has been reported in 1977 as a possible neuromodulator in a study by Schmid-Glenewinkel et al. [51] about its biosynthesis by cadaverine and pipercolic acid in mice. The conversion of lysine into piperidine was observed only in the intestines, probably caused by the intestinal flora, while the formation of cadaverine and pipercolic acid from lysine was observed in the brain, liver, kidney, and large intestine. Pipercolic acid was also formed in the heart. In 1983, Nomura et al. [52] suggested that cadaverine is not a precursor of piperidine in brain, the conversion of pipercolic acid into piperidine in the brain does not constitute a major metabolic pathway, and the main source of piperidine in the CNS may be of nonneural origin. Since 1977, the possible contributions of the diet and the intestinal bacteria to the endogenous pool(s) of piperidine have been also discussed. Today, we agree that piperidine—a microbial metabolite—is a naturally occurring metabolite in the human body (a metabolite of cadaverine, a polyamine found in the intestine of humans and mammals) [<https://hmdb.ca/metabolites/HMDB0034301> (accessed on 9 October 2020, 9 October 2021 and 29 December 2022)].

Our findings agree with Sugimoto et al. who identified piperidine as an oral cancer-specific marker by mass spectrometry-based saliva metabolomics [53]. Saliva is a filtration of blood that can reflect the physiological conditions of the body enabling patient monitoring and the prediction of systemic diseases, while it exhibits diurnal variation and the presence of diverse diagnostic analytes, endogenous plus xenobiotics (similar to blood or urine) [54]. In GBM cell lines, the combination of piperidine or piperidine nitroxide tempol (TPL) with TMZ has resulted in synergistic anti-proliferative action [55]. Of note, a piperidine derivative targeting EZH2 (enhancer of zeste homologue 2) has been reported to reduce GBM cell viability and impair tumor development and aggressiveness via an immunomodulatory mechanism [56]. EZH2 is a S-adenosyl-L-methionine (SAM)-dependent methyltransferase, and its role as an epigenetic modulator in different types of cancer has been widely investigated. In GBM, EZH2 overexpression has been correlated with poor prognosis [57,58]. Although little is known about the mechanistic aspects of EZH2 activity in GBM, the inhibition of EZH2 expression by miR-340 in triple negative breast cancer has led to decreased levels of miR-21, revealing a key miRNA network pathway [59]. In our previous study, we have established a 3-miRNA (hsa-miR-20a, hsa-miR-21, hsa-miR-10a)

signature which was able to discriminate low- and high-risk GBM patients, as lower expression levels of miR-21 as well as miR-20a and miR-10a were associated with favorable prognosis [41]. Building on the GBM epigenome-metabolome interplay, we propose a piperidine-EZH2-miR340 mechanistic link—which we have yet to prove.

Taking into account the crosstalk of epigenetic and metabolic signaling in GBM [60], we also noted higher levels of 7-ketocholesterol in the plasma metabolome of low-risk patients (Figure 1). The reprogramming of lipid and cholesterol metabolism has been linked to many cancers, including GBM, while GBM cell growth is highly dependent on cholesterol. Oxysterols, such as 7-ketocholesterol, are oxidized forms of cholesterol that participate in the regulation of cholesterol metabolism through liver X receptors (LXRs) and sterol regulatory element-binding proteins (SREBPs) [61–64]. SREBPs are highly upregulated in GBM. Furthermore, the feedback loop of miR-29-SCAP/SREBP-1 modulates GBM growth, which is driven by EGFR signaling via the regulation of cholesterol synthesis [65,66]. Oxysterols have been also reported to have antitumor activity in GBM by activating LXRs, thus disrupting cholesterol homeostasis [62]. Our mixed-methods content analysis revealed no output for 2-acetyl-4-methylpyridine, piperidine, and 3-(4-methyl-3-pentenyl) thiophene or hippuric acid. For the latter, however, the study of Mallafré-Muro et al. [67] survived some of our multiple levels of interrogation, according to which low levels of hippuric acid are detected in urine samples of colorectal cancer patients.

Among key pathway perturbations, half of the highly enriched and statistically significant pathways relate to amino acid metabolism, namely tryptophan and arginine/proline metabolism (Figure 3). Our findings align with what reported so far. Amino acid metabolism was found disrupted following a nuclear magnetic resonance (NMR)-based metabolomic analysis in plasma samples of glioma patients and healthy controls [68]. The decreased plasma levels of various amino acids in glioma patients may indicate an increased demand for amino acids at the tumor niche [68–70]. Synergistically to amino acid metabolism and, in particular, arginine/proline metabolism, the dysregulation of nitrogen and/or pyrimidine metabolism pathways may reflect urea cycle dysregulation, providing essential substrates for tumor proliferation and growth [71,72]. As also suggested by Shen et al. arginine, methionine, and kynurenate were found to be significantly associated with two-year overall and disease-free survival in GBM, indicating the prognostic role of these metabolites [22]. Additionally, glutamine, ornithine, tyrosine, and urea were identified in a serum metabolomic analysis in GBM patients, post-treatment [24].

Interrogating the predictive ability of GBM plasma metabolotypes alone (Figure 4) or upon their integration with miRNA data (hsa-miR-20a, hsa-miR-21, hsa-miR-10a) (Figures S3 and S4) [41], both supervised and unsupervised analyses agreed on the predictive value of perlolyrine, piperidine, hippuric acid, 2,6-diisopropyl-3-methylphenol, dopamine, and ( $\pm$ )-(Z)-2-(5-Tetradecenyl) cyclobutanone.

Overall, such key pathway perturbations have been already identified as subjects of epigenetic modulators [60,73]. To our knowledge, only a few studies to date have interrogated GBM plasma metabolotypes in well-balanced cohorts at diagnosis and during follow-up (RT + TMZ) by liquid chromatography mass spectrometry (LC-MS), an analytical platform of high sensitivity, as performed herein. Even fewer are those that seek for a combinatorial space of molecular interactions and contexts with emphasis on the epigenome-metabolome interplay. To us, this is where answers to challenging questions are to be found. Why healthy cells acquire and sustain cancer phenotypes? Do canonical driver mutations truly drive tumor development, or do they reflect environmental influences toward clonal selection, and hence, such mutations provide a fitness advantage? At every biological layer investigated so far, cancer cells exhibit dysregulated behavior [74], while emerging datasets suggest that molecular and phenotypic alterations are highly heterogeneous across patients or cancer types or even within the tumor itself [75]. Cancer metabolotypes are known to be closer to cellular phenotypes and, thus, provide a more functional understanding of cellular states and transitions. Why? Metabolism is a dynamic

process; there is a constant catalysis of metabolic reactions, during which reaction rates and metabolite abundance (intracellular and extracellular) define a metabolic state.

## 5. Conclusions

Our results point to the role of metabolic remodeling in GBM plasticity and disease severity via bioenergetic profiles that map patterns and shed light upon GBM biology and RT + TMZ response. GBM plasma metabolotypes alone or upon miRNA data integration are of predictive value, as shown by both supervised and unsupervised analyses. An in-depth understanding of aberrant metabolism promises to provide the framework for personalized metabolic modulation, in particular when the GBM epigenome-metabolome interplay is considered. We envisage that this is how drug repurposing in translational precision medicine will be of benefit [76]: right drug, right dose, right patient (when also timing is right).

**Supplementary Materials:** The following supporting information can be downloaded at: <https://www.mdpi.com/article/10.3390/metabo13030362/s1>, Table S1. Demographic and clinical characteristics of the standard-of-care treated GBM patients; Table S2. Performance metrics in 10-fold cross validation process for the four models trained to classify low- and high-risk patients when metabolotypes are considered; Table S3. Confusion matrix of each of the classifiers tested (correct and false predictions per model are shown following a 10-fold cross validation); Figure S1. Prediction accuracy during recursive feature elimination process (based on metabolotypes); Figure S2. Variable importance analysis (Gradient Boosting); Figure S3. Scatter plot of patients clustered by k-means algorithm based on miRNA expression levels and metabolotypes; Figure S4. Hierarchical clustering dendrogram for the low- and high-risk groups based on miRNA expression levels and metabolotypes.

**Author Contributions:** Conceptualization, T.K.; methodology, V.B., S.O. and E.S.; sample collection, A.T. and I.M.G.; validation, V.B.; formal analysis, V.B.; software, V.B., S.O.; investigation, V.B., E.S. and S.O.; resources, D.K., V.Z. and T.K.; data curation, V.B.; writing—original draft preparation, V.B. and T.K.; writing—review and editing, V.B., S.O., E.S., I.M.G., A.T., V.P., V.Z., D.K. and T.K.; visualization, V.B. and S.O.; supervision, V.Z., V.P., D.K. and T.K.; funding acquisition, T.K. All authors have read and agreed to the published version of the manuscript.

**Funding:** This research is supported by the European Regional Development Fund of the European Union and Greek national funds through the Operational Program Competitiveness, Entrepreneurship and Innovation, under the call RESEARCH—CREATE—INNOVATE (project code: T2EDK-03153).

**Institutional Review Board Statement:** The study protocol is in accordance with the Declaration of Helsinki and has been approved by the ethics review board of the General University Hospital of Patras, Greece. IRB protocol number: 8735/142 (9 February 2021).

**Informed Consent Statement:** Written informed consent was obtained from all subjects involved in the study.

**Data Availability Statement:** All data generated or analyzed during this study are included in this published article and its supplementary information files.

**Acknowledgments:** The authors would like to thank the institutions and volunteers who took part in the study. We also wish to acknowledge Maria Pittaka for sample collection.

**Conflicts of Interest:** The authors declare no conflict of interest. The funders had no role in the design of the study; in the collection, analyses, or interpretation of data; in the writing of the manuscript, or in the decision to publish the results.

## References

1. Nguyen, T.T.T.; Zhang, Y.; Shang, E.; Shu, C.; Torrini, C.; Zhao, J.; Bianchetti, E.; Mela, A.; Humala, N.; Mahajan, A.; et al. HDAC Inhibitors Elicit Metabolic Reprogramming by Targeting Super-Enhancers in Glioblastoma Models. *J. Clin. Investig.* **2020**, *130*, 3699–3716. [CrossRef] [PubMed]
2. Yabo, Y.A.; Niclou, S.P.; Golebiewska, A. Cancer Cell Heterogeneity and Plasticity: A Paradigm Shift in Glioblastoma. *Neuro Oncol.* **2022**, *24*, 669–682. [CrossRef] [PubMed]

3. Louis, D.N.; Perry, A.; Wesseling, P.; Brat, D.J.; Cree, I.A.; Figarella-Branger, D.; Hawkins, C.; Ng, H.K.; Pfister, S.M.; Reifenberger, G.; et al. The 2021 WHO Classification of Tumors of the Central Nervous System: A Summary. *Neuro Oncol.* **2021**, *23*, 1231–1251. [[CrossRef](#)] [[PubMed](#)]
4. Stupp, R.; Mason, W.P.; van den Bent, M.J.; Weller, M.; Fisher, B.; Taphoorn, M.J.B.; Belanger, K.; Brandes, A.A.; Marosi, C.; Bogdahn, U.; et al. Radiotherapy plus Concomitant and Adjuvant Temozolomide for Glioblastoma. *N. Engl. J. Med.* **2005**, *352*, 987–996. [[CrossRef](#)]
5. Stupp, R.; Brada, M.; van den Bent, M.J.; Tonn, J.C.; Pentheroudakis, G. High-Grade Glioma: ESMO Clinical Practice Guidelines for Diagnosis, Treatment and Follow-Up. *Ann. Oncol.* **2014**, *25*, 93–101. [[CrossRef](#)]
6. Bai, H.; Harmanci, A.S.; Eron-Omay, E.Z.; Li, J.; Coşkun, S.; Simon, M.; Krischek, B.; Özdoğan, K.; Omay, S.B.; Sorensen, E.A.; et al. Integrated genomic characterization of IDH1-mutant glioma malignant progression. *Nat. Genet.* **2016**, *48*, 59–66. [[CrossRef](#)]
7. Pentsova, E.I.; Shah, R.H.; Tang, J.; Boire, A.; You, D.; Briggs, S.; Omuro, A.; Lin, X.; Fleisher, M.; Grommes, C.; et al. Evaluating cancer of the central nervous system through next-generation sequencing of cerebrospinal fluid. *J. Clin. Oncol.* **2016**, *34*, 2404–2415. [[CrossRef](#)]
8. Cohen, J.D.; Li, L.; Wang, Y.; Thoburn, C.; Afsari, B.; Danilova, L.; Douville, C.; Javed, A.A.; Wong, F.; Mattox, A.; et al. Detection and localization of surgically resectable cancers with a multi-analyte blood test. *Science* **2018**, *359*, 926–930. [[CrossRef](#)]
9. Lennon, A.M.; Buchanan, A.H.; Kinde, I.; Warren, A.; Honushesky, A.; Cohain, A.T.; Ledbetter, D.H.; Sanfilippo, F.; Sheridan, K.; Rosica, D.; et al. Feasibility of blood testing combined with PET-CT to screen for cancer and guide intervention. *Science* **2020**, *369*, eabb9601. [[CrossRef](#)]
10. Won, W.-J.; Deshane, J.S.; Leavenworth, J.W.; Oliva, C.R.; Griguer, C.E. Metabolic and Functional Reprogramming of Myeloid-Derived Suppressor Cells and Their Therapeutic Control in Glioblastoma. *Cell Stress* **2019**, *3*, 47–65. [[CrossRef](#)]
11. Broekman, M.L.; Maas, S.L.N.; Abels, E.R.; Mempel, T.R.; Krichevsky, A.M.; Breakefield, X.O. Multidimensional communication in the microenvirons of glioblastoma. *Nat. Rev. Neurol.* **2018**, *14*, 482–495. [[CrossRef](#)] [[PubMed](#)]
12. Gilard, V.; Ferey, J.; Marguet, F.; Fontanilles, M.; Ducatez, F.; Pilon, C.; Lesueur, C.; Pereira, T.; Basset, C.; Schmitz-Afonso, I.; et al. Integrative Metabolomics Reveals Deep Tissue and Systemic Metabolic Remodeling in Glioblastoma. *Cancers* **2021**, *13*, 5157. [[CrossRef](#)] [[PubMed](#)]
13. Huang, J.; Weinstein, S.J.; Kitahara, C.M.; Karoly, E.D.; Sampson, J.N.; Albanes, D. A Prospective Study of Serum Metabolites and Glioma Risk. *Oncotarget* **2017**, *8*, 70366–70377. [[CrossRef](#)] [[PubMed](#)]
14. Dong, Z.; Cui, H. Epigenetic Modulation of Metabolism in Glioblastoma. *Semin. Cancer Biol.* **2019**, *57*, 45–51. [[CrossRef](#)] [[PubMed](#)]
15. Agnihotri, S.; Zadeh, G. Metabolic Reprogramming in Glioblastoma: The Influence of Cancer Metabolism on Epigenetics and Unanswered Questions. *Neuro Oncol.* **2016**, *18*, 160–172. [[CrossRef](#)]
16. Johnson, C.; Warmoes, M.O.; Shen, X.; Locasale, J.W. Epigenetics and cancer metabolism. *Cancer Lett.* **2015**, *356*, 309–314. [[CrossRef](#)]
17. Venneti, S.; Thompson, C.B. Metabolic modulation of epigenetics in gliomas. *Brain Pathol.* **2013**, *23*, 217–221. [[CrossRef](#)]
18. Luan, W.; Wang, Y.; Chen, X.; Shi, Y.; Wang, J.; Zhang, J.; Qian, J.; Li, R.; Tao, T.; Wei, W.; et al. PKM2 promotes glucose metabolism and cell growth in gliomas through a mechanism involving a let-7a/c- Myc/hnRNPA1 feedback loop. *Oncotarget* **2015**, *6*, 13006–13018. [[CrossRef](#)]
19. Liu, Z.; Wang, J.; Li, Y.; Fan, J.; Chen, L.; Xu, R. MicroRNA-153 regulates glutamine metabolism in glioblastoma through targeting glutaminase. *Tumour Biol.* **2017**, *39*, 1010428317691429. [[CrossRef](#)]
20. Alfaridus, H.; de los Angeles Estevez-Cabrero, M.; Rowlinson, J.; Aboalmaaly, A.; Lourdasamy, A.; Abdelrazig, S.; Ortori, C.; Grundy, R.; Kim, D.H.; McIntyre, A.; et al. Intratumour Heterogeneity in MicroRNAs Expression Regulates Glioblastoma Metabolism. *Sci. Rep.* **2021**, *11*, 15908. [[CrossRef](#)]
21. Kwak, S.; Park, S.H.; Kim, S.H.; Sung, G.J.; Song, J.H.; Jeong, J.H.; Kim, H.; Ha, C.H.; Kim, S.W.; Choi, K.C. MiR-3189-Targeted GLUT3 Repression by HDAC2 Knockdown Inhibits Glioblastoma Tumorigenesis through Regulating Glucose Metabolism and Proliferation. *J. Exp. Clin. Cancer Res.* **2022**, *41*, 87. [[CrossRef](#)] [[PubMed](#)]
22. Shen, J.; Song, R.; Hodges, T.R.; Heimberger, A.B.; Zhao, H. Identification of Metabolites in Plasma for Predicting Survival in Glioblastoma. *Mol. Carcinog.* **2018**, *57*, 1078–1084. [[CrossRef](#)]
23. Rogachev, A.D.; Alesanov, N.A.; Ivanisenko, V.A.; Ivanisenko, N.V.; Gaisler, E.V.; Oleshko, O.S.; Cheresiz, S.V.; Mishinov, S.V.; Stupak, V.V.; Pokrovsky, A.G. Correlation of Metabolic Profiles of Plasma and Cerebrospinal Fluid of High-Grade Glioma Patients. *Metabolites* **2021**, *11*, 133. [[CrossRef](#)] [[PubMed](#)]
24. Mörén, L.; Wibom, C.; Bergström, P.; Johansson, M.; Antti, H.; Bergenheim, A.T. Characterization of the Serum Metabolome Following Radiation Treatment in Patients with High-Grade Gliomas. *Radiat. Oncol.* **2016**, *11*, 51. [[CrossRef](#)] [[PubMed](#)]
25. Baranovičová, E.; Galanda, T.; Galanda, M.; Hatok, J.; Kolarovszki, B.; Richterová, R.; Račay, P. Metabolomic Profiling of Blood Plasma in Patients with Primary Brain Tumours: Basal Plasma Metabolites Correlated with Tumour Grade and Plasma Biomarker Analysis Predicts Feasibility of the Successful Statistical Discrimination from Healthy Subjects—A Preliminary Study. *IUBMB Life* **2019**, *71*, 1994–2002. [[CrossRef](#)]
26. Amara, A.; Frainay, C.; Jourdan, F.; Naake, T.; Neumann, S.; Novoa-del-Toro, E.M.; Salek, R.M.; Salzer, L.; Scharfenberg, S.; Witting, M. Networks and graphs discovery in metabolomics data analysis and interpretation. *Front. Mol. Biosci.* **2022**, *9*, 841373. [[CrossRef](#)]

27. Zhou, J.; Ji, N.; Wang, G.; Zhang, Y.; Song, H.; Yuan, Y.; Yanhg, C.; Jin, Y.; Zhang, Z.; Zhnag, L.; et al. Metabolic detection of malignant brain gliomas through plasma lipidomic analysis and support vector machine-based machine learning. *EBioMedicine* **2022**, *81*, 104097. [[CrossRef](#)] [[PubMed](#)]
28. Wishart, D.S.; Guo, A.; Oler, E.; Wang, F.; Anjum, A.; Peters, H.; Dizon, R.; Sayeeda, Z.; Tian, S.; Lee, B.L.; et al. HMDB 5.0: The Human Metabolome Database for 2022. *Nucleic Acids Res.* **2022**, *50*, D622–D631. [[CrossRef](#)]
29. Haug, K.; Cochrane, K.; Nainala, V.C.; Williams, M.; Chang, J.; Jayaseelan, K.V.; O'Donovan, C. MetaboLights: A resource evolving in response to the needs of its scientific community. *Nucleic Acids Res.* **2020**, *48*, D440–D444. [[CrossRef](#)]
30. Louis, D.N.; Perry, A.; Reifenberger, G.; von Deimling, A.; Figarella-Branger, D.; Cavenee, W.K.; Ohgaki, H.; Wiestler, O.D.; Kleihues, P.; Ellison, D.W. The 2016 World Health Organization Classification of Tumors of the Central Nervous System: A Summary. *Acta Neuropathol.* **2016**, *131*, 803–820. [[CrossRef](#)]
31. Chalikiopoulou, C.; Gómez-Tamayo, J.C.; Katsila, T. Untargeted metabolomics for disease-specific signatures. *Methods Mol. Biol.* **2023**, *2571*, 71–81. [[CrossRef](#)] [[PubMed](#)]
32. Adusumilli, R.; Mallick, P. Data Conversion with ProteoWizard MsConvert. *Methods Mol. Biol.* **2017**, *1550*, 339–368. [[CrossRef](#)] [[PubMed](#)]
33. Pang, Z.; Chong, J.; Zhou, G.; de Lima Morais, D.A.; Chang, L.; Barrette, M.; Gauthier, C.; Jacques, P.É.; Li, S.; Xia, J. MetaboAnalyst 5.0: Narrowing the Gap between Raw Spectra and Functional Insights. *Nucleic Acids Res.* **2021**, *49*, W388–W396. [[CrossRef](#)] [[PubMed](#)]
34. Li, S.; Park, Y.; Duraisingham, S.; Strobel, F.H.; Khan, N.; Soltow, Q.A.; Jones, D.P.; Pulendran, B. Predicting network activity from high throughput metabolomics. *PLoS Comput. Biol.* **2013**, *9*, e1003123. [[CrossRef](#)]
35. Guyon, I.; Weston, J.; Barnhill, S.; Vapnik, V. Gene selection for cancer classification using support vector machines. *Mach. Learn.* **2002**, *46*, 389–422. [[CrossRef](#)]
36. Cortes, C.; Vapnik, V. Support-vector networks. *Mach. Learn.* **1995**, *20*, 273–297. [[CrossRef](#)]
37. Liaw, A.; Wiener, M. Classification and Regression by Random Forest. *R News* **2002**, *2*, 18–22.
38. Chen, C.; Guestrin, C. XGBoost: A scalable tree boosting system. In Proceedings of the 22nd ACM SIGKDD International Conference on Knowledge Discovery and Data Mining, San Francisco, CA, USA, 13–17 August 2016; pp. 785–794. [[CrossRef](#)]
39. Friedman, J. Stochastic gradient boosting. *Comput. Stat. Data Anal.* **2002**, *38*, 367–378. [[CrossRef](#)]
40. Kuhn, M. Building Predictive Models in R Using the caret Package. *J. Stat. Softw.* **2008**, *28*, 1–26. [[CrossRef](#)]
41. Bafiti, V.; Ouzounis, S.; Chalikiopoulou, C.; Grigorakou, E.; Grypari, I.M.; Gregoriou, G.; Theofanopoulos, A.; Panagiotopoulos, V.; Prodromidi, E.; Cavouras, D.; et al. A 3-MiRNA Signature Enables Risk Stratification in Glioblastoma Multiforme Patients with Different Clinical Outcomes. *Curr. Oncol.* **2022**, *29*, 4315–4331. [[CrossRef](#)]
42. Lloyd, S. Least squares quantization in PCM. *IEEE Trans. Inf. Theory* **1982**, *28*, 129–137. [[CrossRef](#)]
43. Jain, A.K.; Murty, M.N.; Flynn, P.J. Data clustering: A review. *ACM Comput. Surv.* **1999**, *31*, 264–323. [[CrossRef](#)]
44. Uribe, D.; Niechi, I.; Rackov, G.; Erices, J.I.; Martín, R.S.; Quezada, C. Adapt to Persist: Glioblastoma Microenvironment and Epigenetic Regulation on Cell Plasticity. *Biology* **2022**, *11*, 313. [[CrossRef](#)]
45. Pandey, R.; Cafilisch, L.; Lodi, A.; Brenner, A.J.; Tiziani, S. Metabolomic Signature of Brain Cancer. *Mol. Carcinog.* **2017**, *56*, 2355–2371. [[CrossRef](#)] [[PubMed](#)]
46. Ballman, K.V.; Buckner, J.C.; Brown, P.D.; Giannini, C.; Flynn, P.J.; Laplant, B.R.; Jaeckle, K.A.; Ballman, K.; Clinic, M. Neuro-oncology The Relationship between Six-Month Progression-Free Survival and 12-Month Overall Survival End Points for Phase II Trials in Patients with Glioblastoma Multiforme. *USA Neuro-Oncol.* **2007**, *9*, 29–38. [[CrossRef](#)] [[PubMed](#)]
47. Kudulaiti, N.; Zhou, Z.; Luo, C.; Zhang, J.; Zhu, F.; Wu, J. A Nomogram for Individualized Prediction of Overall Survival in Patients with Newly Diagnosed Glioblastoma: A Real-World Retrospective Cohort Study. *BMC Surg.* **2021**, *21*, 238. [[CrossRef](#)] [[PubMed](#)]
48. Chahal, M.; Thiessen, B.; Mariano, C. Treatment of Older Adult Patients with Glioblastoma: Moving towards the Inclusion of a Comprehensive Geriatric Assessment for Guiding Management. *Curr. Oncol.* **2022**, *29*, 360–376. [[CrossRef](#)] [[PubMed](#)]
49. Zhu, F.; Patumcharoenpol, P.; Zhang, C.; Yang, Y.; Chan, J.; Meechai, A.; Vongsangnak, W.; Shen, B. Biomedical text mining and its applications in cancer research. *J. Biomed. Inform.* **2013**, *46*, 200–211. [[CrossRef](#)] [[PubMed](#)]
50. Moreno, P.; Jayaseelan, K.V.; Stenibeck, C. Towards automated metabolome assembly: Application of text mining to correlate small molecules, targets and tissues. *J. Cheminform.* **2011**, *3* (Suppl. 1), 19. [[CrossRef](#)]
51. Schmidt-Glenewinkel, T.; Nomura, Y.; Giacobini, E. The conversion of lysine into piperidine, cadaverine, and pipercolic acid in the brain and other organs of the mouse. *Neurochem. Res.* **1977**, *2*, 619–637. [[CrossRef](#)]
52. Nomura, Y.; Schmidt-Glenewinkel, T.; Giacobini, E.; Ortiz, J. Metabolism of cadaverine and pipercolic acid in brain and other organs of the mouse. *J. Neurosci. Res.* **1983**, *9*, 279–289. [[CrossRef](#)]
53. Sugimoto, M.; Wong, D.T.; Hirayama, A.; Soga, T.; Tomita, M. Capillary electrophoresis mass spectrometry-based saliva metabolomics identified oral, breast and pancreatic cancer-specific profiles. *Metabolomics* **2010**, *6*, 78–95. [[CrossRef](#)]
54. Ishikawa, S.; Sugimoto, M.; Kitabatake, K.; Sugano, A.; Nakamura, M.; Kaneko, M.; Ota, S.; Hiwatari, K.; Enomoto, A.; Soga, T.; et al. Identification of salivary metabolomic biomarkers for oral cancer screening. *Sci. Rep.* **2016**, *6*, 31520. [[CrossRef](#)] [[PubMed](#)]
55. Ravizza, R.; Cereda, E.; Monti, E.; Gariboldi, M.B. The Piperidine Nitroxide Tempol Potentiates the Cytotoxic Effects of Temozolomide in Human Glioblastoma Cells. *Int. J. Oncol.* **2004**, *25*, 1817–1822. [[CrossRef](#)] [[PubMed](#)]

56. Stazi, G.; Taglieri, L.; Nicolai, A.; Romanelli, A.; Fioravanti, R.; Morrone, S.; Sabatino, M.; Ragno, R.; Taurone, S.; Nebbioso, M.; et al. Dissecting the Role of Novel EZH2 Inhibitors in Primary Glioblastoma Cell Cultures: Effects on Proliferation, Epithelial-Mesenchymal Transition, Migration, and on the pro-Inflammatory Phenotype. *Clin. Epigenet.* **2019**, *11*, 173. [[CrossRef](#)] [[PubMed](#)]
57. Viré, E.; Brenner, C.; Deplus, R.; Blanchon, L.; Fraga, M.; Didelot, C.; Morey, L.; van Eynde, A.; Bernard, D.; Vanderwinden, J.M.; et al. The Polycomb Group Protein EZH2 Directly Controls DNA Methylation. *Nature* **2006**, *439*, 871–874. [[CrossRef](#)] [[PubMed](#)]
58. del Moral-Morales, A.; González-Orozco, J.C.; Hernández-Vega, A.M.; Hernández-Ortega, K.; Peña-Gutiérrez, K.M.; Camacho-Arroyo, I. EZH2 Mediates Proliferation, Migration, and Invasion Promoted by Estradiol in Human Glioblastoma Cells. *Front. Endocrinol.* **2022**, *13*, 66. [[CrossRef](#)]
59. Shi, Z.; Li, Y.; Qian, X.; Hu, Y.; Liu, J.; Zhang, S.; Zhang, J. MiR-340 Inhibits Triple-Negative Breast Cancer Progression by Reversing EZH2 Mediated miRNAs Dysregulated Expressions. *J. Cancer* **2017**, *8*, 3037–3048. [[CrossRef](#)]
60. Marouli, M.; Strepkos, D.; Papavassiliou, K.A.; Papavassiliou, A.G.; Piperi, C. Crosstalk of epigenetic and metabolic signaling underpinning glioblastoma pathogenesis. *Cancers* **2022**, *14*, 2655. [[CrossRef](#)]
61. Han, M.; Wang, S.; Yang, N.; Wang, X.; Zhao, W.; Saed, H.S.; Daubon, T.; Huang, B.; Chen, A.; Li, G.; et al. Therapeutic Implications of Altered Cholesterol Homeostasis Mediated by Loss of CYP46A1 in Human Glioblastoma. *EMBO Mol. Med.* **2020**, *12*, e10924. [[CrossRef](#)]
62. Guo, X.; Zhou, S.; Yang, Z.; Li, Z.A.; Hu, W.; Dai, L.; Liang, W.; Wang, X. Cholesterol Metabolism and Its Implication in Glioblastoma Therapy. *J. Cancer* **2022**, *13*, 1745. [[CrossRef](#)]
63. Nury, T.; Zarrouk, A.; Yammine, A.; Mackrill, J.J.; Vejux, A.; Lizard, G. Oxidative cell death: A Type of Cell Death Induced by Some Oxysterols. *Br. J. Pharmacol.* **2021**, *178*, 3115–3123. [[CrossRef](#)] [[PubMed](#)]
64. Villa, G.R.; Hulce, J.J.; Zanca, C.; Bi, J.; Ikegami, S.; Cahill, G.L.; Gu, Y.; Lum, K.M.; Masui, K.; Yang, H.; et al. An LXR-Cholesterol Axis Creates a Metabolic Co-Dependency for Brain Cancers. *Cancer Cell* **2016**, *30*, 683. [[CrossRef](#)] [[PubMed](#)]
65. Ru, P.; Hu, P.; Geng, F.; Mo, X.; Cheng, C.; Yoo, J.Y.; Cheng, X.; Wu, X.; Guo, J.Y.; Nakano, I.; et al. Feedback loop regulation of SCAP/SREBP-1 by miR-29 modulates EGFR signaling-driven glioblastoma growth. *Cell Rep.* **2016**, *16*, 1527–1535. [[CrossRef](#)] [[PubMed](#)]
66. Ru, P.; Guo, D. microRNA-29 mediates a novel negative feedback loop to regulate SCAP/SREBP-1 and lipid metabolism. *RNA Dis.* **2017**, *4*, e1525. [[CrossRef](#)]
67. Mallafre-Muro, C.; Llambrich, M.; Cumeras, R.; Pardo, A.; Brezmes, J.; Marco, S.; Gumà, J. Comprehensive Volatilome and Metabolome Signatures of Colorectal Cancer in Urine: A Systematic Review and Meta-Analysis. *Cancers* **2021**, *13*, 2534. [[CrossRef](#)]
68. Cuperlovic-Culf, M.; Ferguson, D.; Culf, A.; Morin, P., Jr.; Touaibia, M. 1H NMR metabolomics analysis of glioblastoma subtypes: Correlation between metabolomics and gene expression characteristics. *J. Biol. Chem.* **2012**, *287*, 20164–20175. [[CrossRef](#)]
69. Bobeff, E.J.; Szczesna, D.; Bieńkowski, M.; Janczar, K.; Chmielewska-Kassassir, M.; Wiśniewski, K.; Papierz, W.; Wozniak, L.A.; Jaskólski, D.J. Plasma Amino Acids Indicate Glioblastoma with ATRX Loss. *Amino Acids* **2021**, *53*, 119–132. [[CrossRef](#)]
70. Chen, S.; Jiang, J.; Shen, A.; Miao, Y.; Cao, Y.; Zhang, Y.; Cong, P.; Gao, P. Rewired Metabolism of Amino Acids and Its Roles in Glioma Pathology. *Metabolites* **2022**, *12*, 918. [[CrossRef](#)]
71. Semreen, A.M.; Alsoud, L.O.; El-Huneidi, W.; Ahmed, M.; Bustanji, Y.; Abu-Gharbieh, E.; El-Awady, R.; Ramadan, W.S.; Alqudah, M.A.Y.; Shara, M.; et al. Metabolomics Analysis Revealed Significant Metabolic Changes in Brain Cancer Cells Treated with Paclitaxel and/or Etoposide. *Int. J. Mol. Sci.* **2022**, *23*, 13940. [[CrossRef](#)]
72. Keshet, R.; Szlosarek, P.; Carracedo, A.; Erez, A. Rewiring Urea Cycle Metabolism in Cancer to Support Anabolism. *Nat. Rev. Cancer* **2018**, *18*, 634–645. [[CrossRef](#)] [[PubMed](#)]
73. Tribe, A.K.W.; McConnell, M.J.; Teesdale-Spittle, P.H. The Big Picture of Glioblastoma Malignancy: A Meta-Analysis of Glioblastoma Proteomics to Identify Altered Biological Pathways. *ACS Omega* **2021**, *6*, 24535–24544. [[CrossRef](#)] [[PubMed](#)]
74. Hanahan, D.; Weinberg, R.A. Hallmarks of cancer: The next generation. *Cell* **2011**, *144*, 646–674. [[CrossRef](#)] [[PubMed](#)]
75. Gonçalves, E.; Frezza, C. Genome and metabolome: Chance and necessity. *Genome Biol.* **2021**, *22*, 276. [[CrossRef](#)] [[PubMed](#)]
76. Hartl, D.; de Luca, V.; Kostikova, A.; Laramie, J.; Kennedy, S.; Ferrero, E.; Siegel, R.; Fink, M.; Ahmed, S.; Millholland, J.; et al. Translational precision medicine: An industry perspective. *J. Transl. Med.* **2021**, *19*, 245. [[CrossRef](#)]

**Disclaimer/Publisher's Note:** The statements, opinions and data contained in all publications are solely those of the individual author(s) and contributor(s) and not of MDPI and/or the editor(s). MDPI and/or the editor(s) disclaim responsibility for any injury to people or property resulting from any ideas, methods, instructions or products referred to in the content.